

Strong dependence of magnon diffusion in $\text{Y}_3\text{Fe}_5\text{O}_{12}$ on light excitation

Shuanhu Wang¹, Gang Li², Erjia Guo³, Yang Zhao¹, Jianyuan Wang¹, Lvquan Zou⁴, Hong Yan¹, Jianwang Cai², Zhaoting Zhang¹, Min Wang¹, Yingyi Tian¹, Xiaoli Zheng², Jirong Sun^{2*}, Kexin Jin^{1*}

1) Shanxi Key Laboratory of Condensed Matter Structures and Properties, School of Science, Northwestern Polytechnical University, Xi'an 710072, China

2) Beijing National Laboratory for Condensed Matter and Institute of Physics, Chinese Academy of Sciences, Beijing 100190, China

3) Quantum Condensed Matter Division, Oak Ridge National Laboratory, Oak Ridge, TN 37831, USA

4) High Magnetic Field Laboratory, Chinese Academy of Science, 230031 Hefei China

*e-mail: jrsun@iphy.ac.cn; jinkx@nwpu.edu.cn

Abstract

Tuning the transport behavior of magnons may lead to an energy-efficient technology for information transmission and processing. This stimulates intensive investigations on $\text{Y}_3\text{Fe}_5\text{O}_{12}$ (YIG) that exhibits the longest magnon diffusion distance among magnetic materials. While most of the previous works focused on the determination of magnon diffusion length by various techniques, herein we demonstrated how to tune magnon diffusion by laser excitation. We found that the diffusion length is strongly dependent on laser wavelength when the magnon is generated by exposing YIG directly to laser beam. The diffusion length, determined by a nonlocal geometry at room temperature, is $\sim 30 \mu\text{m}$ for the magnons produced by visible light (400-650 nm), and $\sim 160\text{-}180 \mu\text{m}$ for the laser between 808 nm and 980 nm. The diffusion distance is much longer than the reported value. In addition to thermal gradient, we found that light illumination affected the electron configuration of the Fe^{3+} ion in YIG. Long wavelength laser triggers a high spin to low spin state transition of the Fe^{3+} ions in FeO_6 octahedra. This in turn causes a substantial softening of the magnon thus a dramatic increase in diffusion distance. The present work paves the way towards an efficient tuning

of magnon transport behavior which is crucially important for magnon spintronics.

Introduction

Magnons describe the deviation of a magnetic system from a fully magnetic order. Based on spin Seebeck effect (SSE)¹, non-equilibrium magnons can be generated by a thermal gradient across a magnet. The diffusion of these magnons forms magnon current or spin current. By injecting spin current into a heavy metal¹⁻³ or a topological insulator⁴, which has a strong spin-orbit coupling thus a strong inverse spin Hall effect (ISHE), it can be converted into charge current thus easily detected. The SSE has been observed in a wide range of materials, including ferromagnetic¹, ferri-magnetic⁵, anti-ferromagnetic⁶ and even some paramagnetic materials⁷. However, the diffusion length of the non-equilibrium magnon is still in hot debate. A recent report showed that the SSE first grew and then saturated as the film thickness of $\text{Y}_3\text{Fe}_5\text{O}_{12}$ (YIG) increased⁸. At room temperature, the characteristic thickness for the SSE-saturation is $\sim 1 \mu\text{m}$ for liquid-phase epitaxy-grown YIG and $\sim 0.1 \mu\text{m}$ for pulsed laser deposited YIG. Using laser illumination to locally break the thermal equilibrium between magnons and phonons, which can be probed directly by micro-Brillouin light scattering, An *et al.*⁹ found that the magnon diffusion length is $3.1 \mu\text{m}$ around room temperature.

Recently, nonlocal spin Seebeck geometry¹⁰⁻¹⁴ was widely adopted to investigate spin transport behavior; the spatially separated structure makes the measurements immune to parasitic thermoelectric effect^{15, 16}. Through a spin accumulation in Pt in a nonlocal structure, the magnons can be generated and detected in a fully electrical way. The first work in this aspect was done by Cornelissen *et al.* in 2015¹⁰. The authors found that the diffusion length of the non-equilibrium magnon is $\sim 9.4 \mu\text{m}$ at room temperature for the YIG film with thickness of 200 nm. Focusing laser spot on a Pt absorption pad to generate thermal magnons^{11, 17} and detecting the ISHE signals from a Pt bar separated from the laser spot, Giles *et al.* declared that the magnon diffusion length is less than $9 \mu\text{m}$ at room temperature and at least $47 \mu\text{m}$ at 23 K¹¹.

Compared to simply determining diffusion distance, tuning the transport behavior of the magnon, which is highly desired, is obviously much more important

and challenging. Despite the tremendous advances on caloric spintronics, works in this regard are scarce. As well established, the transport behavior of the magnon strongly depends on dispersion relation. Earlier investigations on optical spectra showed that the electron configuration of the Fe^{3+} ions in YIG can be affected by light excitation^{18,19}. This in turn will affect the dispersion relation of the magnon, due to the change in spin state and superexchange interaction between Fe^{3+} ions. These works suggest a clue to tune magnon diffusion by light excitation rather than the conventional opto-thermal and electro-thermal techniques. Based on a specifically designed nonlocal geometry, we performed a systematic investigation on transport behavior of the magnon in YIG, focusing on how to tune magnon diffusion by laser illumination. Exposing the sample directly to a laser spot, we find diffusion length of the magnon is strongly dependent on the wavelength of excitation light. The diffusion distance is ~ 30 μm when induced by visible light (405-650 nm), and ~ 160 -180 μm when light wavelength is between 808 nm and 980 nm. Therefore, the laser excitation causes not only thermal gradient but also induces the electron configuration transition of the Fe^{3+} ions in YIG, and then modifies the dispersion relation and the diffusion distance.

Experiment

At first, the YIG films were grown on (111)-oriented $\text{Gd}_3\text{Ga}_5\text{O}_{12}$ (GGG) substrates ($5 \times 3 \times 0.5$ mm³) by the techniques of pulsed laser deposition (PLD) and liquid phase epitaxy (LPE), respectively, with the corresponding film thicknesses of 40 nm and 20 μm . Then a Pt layer with a thickness of 5 nm was deposited by magnetron sputtering on YIG through a bar-shaped mask. The size of Pt strip was 4.8×0.5 mm². The surface morphology of YIG was measured by atomic force microscopy (Supplementary Fig. S1), which shows a root mean square roughness of 1.2 Å (PLD sample) or 1.1 nm (LPE sample). Smooth surface is expected to favor a high spin mixing conductance at the Pt-YIG interface²⁰. X-ray diffraction (XRD) analysis confirmed the epitaxial growth of YIG on GGG and the high film quality, as indicated by the sharp (444) reflection and the appearance of interference peaks

(Supplementary Fig. S2). The film thickness of YIG (PLD sample) and Pt was determined by low-angle X-ray reflectivity. Further details on sample preparations and characterizations can be found in Supplementary materials.

Magnetic field (H) was provided by two Helmholtz coils, applied along the x -axis of the sample. Two electrodes aligning along the y -axis were used to detect the ISHE voltage (V_{ISHE}). The sample was attached to cryostat by silver paste to get well thermal contact and to absorb the transmitted thermal energy from the laser beam. The cryostat is sealed in an electromagnetically shielding box with an optical window. The laser beam with a preset wavelength was focused, through a convex mirror, on sample surface to generate an outside-to-inside thermal gradient. The diameter of the light spot was less than 20 μm , measured through an infrared macro lens. As shown in Fig. 1a, the laser and the convex mirror were mounted on a lead rail along the x -axis, which allows a position tuning in micrometers. The output voltage across the Pt bar was recorded as the laser spot was sweeping through the middle of the Pt bar and the surface of the YIG film, along the x -axis. The ISHE voltage is calculated by $V_{\text{ISHE}}=[V_{\text{ISHE}}(+H)-V_{\text{ISHE}}(-H)]/2$, where $V_{\text{ISHE}}(+H)$ and $V_{\text{ISHE}}(-H)$ are the saturation voltages in two oppositely directed magnetic fields. The maximal magnetic field in this experiment is 120 Oe. It is so small that the influence of the opening Zeeman gap on the thermal magnon can be ignored²¹. For clarity, the V_{ISHE} induced by the laser with the wavelength of λ nm was noted as V_{ISHE}^λ .

Results and discussions

When the top surface of the sample is illuminated by a laser beam, the YIG film will absorb a part of the energy. For the film deposited by LPE, the transmitted energy is very low. So the absorbed power can be directly determined by simultaneously measuring the incident and reflected powers by optical power meters. In general, the absorbed energy will establish an out-of-plane thermal gradient, generating thermal magnons due to the SSE. The thermal magnons will then diffuse laterally towards the Pt bar, yielding an electrical voltage (V_{ISHE}) due to the ISHE. Although an in-plane

thermal gradient could also be produced by the absorbed energy, it will mainly locate at the region of the laser spot and decays rapidly in the lateral direction. As proven by the results of finite-element model (FEM) simulation conducted by Giles *et al*¹¹ and An *et al.*⁹, the temperature of the YIG surface will return to room temperature within 15 μm . Therefore, lateral heat flow should have no detectable effect on the measurement of diffusion length.

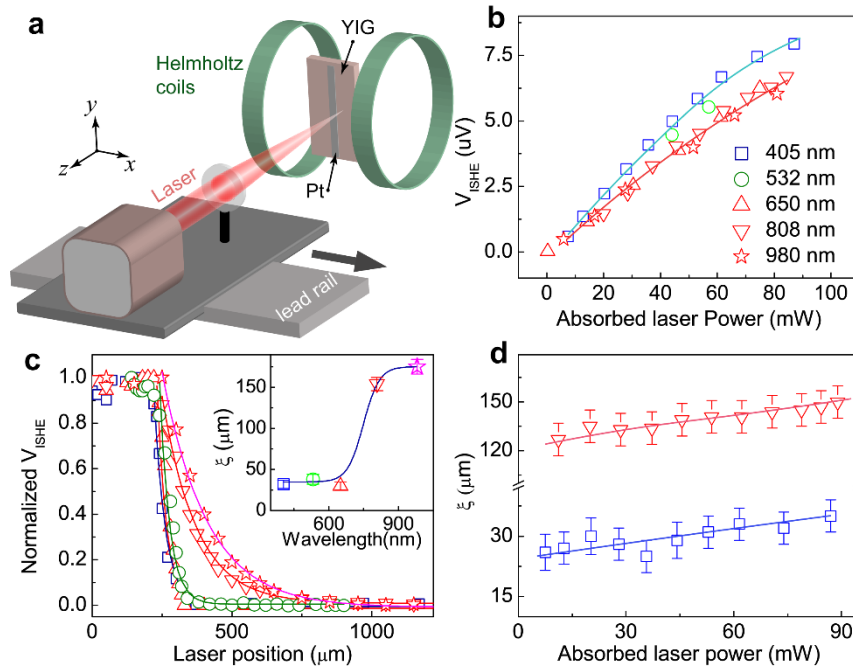


Figure 1 | Dependence of magnon diffusion length on laser wavelength. **a**, The schematic diagram of the experimental setup. **b**, V_{ISHE} as a function of the absorbed laser power, measured with the lasers of different wavelength. Laser spot was positioned at the middle of the Pt bar ($x=0$). **c**, Normalized V_{ISHE} as a function of spot position. Symbols represent the experimental data and solid lines are the results of curve fitting based on Eq. (1). Inset plot shows the diffusion length ξ as a function of laser wavelength, deduced from data fitting. **d**, Dependence of the diffusion length on absorbed laser power. The error bars represent the standard error in the fits. All measurements were conducted at room temperature. Only the data for the YIG prepared by LPE are shown here.

Fig. 1a is a sketch of the experiment setup. Fig. 1b shows the V_{ISHE} as a function of the absorbed laser power. When the laser beam is focused on the middle of the Pt bar, V_{ISHE} linearly increases with laser power as expected. When covering the whole

YIG with a Pt layer (5 nm in thickness), we found that V_{ISHE} remained constant, regardless of the location and size of the laser spot (Supplementary Fig. S2). V_{ISHE}^{405} and V_{ISHE}^{532} are a slightly larger than V_{ISHE}^{808} and V_{ISHE}^{980} . This can be ascribed to the larger absorption coefficient of lights of 405 nm and 532 nm¹⁸.

Fig. 1c presents the dependence of the normalized V_{ISHE} on the position of laser spot. Setting the middle of the Pt electrode to $x=0$, and collecting V_{ISHE} as laser spot sweeps along x -axis, we found that the V_{ISHE} kept nearly constant when laser spot scans across the Pt strip ($-0.25 \text{ mm} < x < 0.25 \text{ mm}$), and exponentially decreased with the distance away from the Pt bar. Fascinatingly, the decay rate strongly depends on wavelength. Illuminated by visible light (405 nm, 532 nm and 605 nm), V_{ISHE} drops to zero immediately when the light spot moves out of the region of the Pt bar. In contrast, it decays slowly with the distance from Pt for the light of 808 nm and 980 nm, remaining sizable when laser spot is 0.5 mm away from the Pt edge. A further analysis indicates that the V_{ISHE}^λ - x relation can be well described by

$$V_{ISHE}^\lambda = V_0^\lambda \exp\left(-\frac{x}{\xi^\lambda}\right) \quad (1)$$

where V_0^λ is a constant and ξ^λ is the diffusion length of the magnons induced by the laser of λ nm. The inset plot in Fig. 1c depicts the magnon diffusion distance as a function of laser wavelength. The thermal magnons induced by long wavelength lasers transport a much longer distance than by short wavelength ones. The diffusion lengths ξ^{405} , ξ^{532} and ξ^{650} are all around 30 μm while ξ^{808} is $\sim 160 \mu\text{m}$ and ξ^{980} is 180 μm . The diffusion length is not sensitive to laser power as shown in Fig. 1d¹¹. There are reports on the diffusion length of thermal magnon determined by different techniques, showing that ξ is generally shorter than several micrometers^{9-11, 22}. The long diffusion length and its strong wavelength dependence observed here indicate that the light not only acts as a heating source to generate thermal gradient but also affects, in some way, the characteristics of the thermal magnon, assigning the latter unconventional diffusion behaviors.

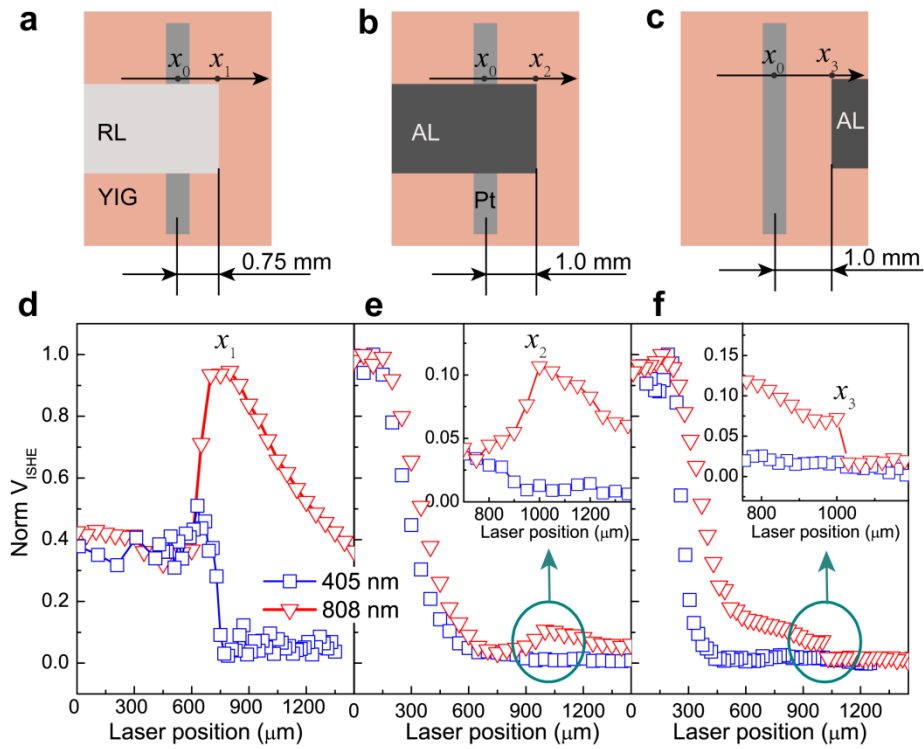


Figure 2 | Experiment for the deeply argument of the wavelength dependent magnon diffusion length. **a**, sample is covered by polished aluminum foil (note as RL) to reflect the injected laser. **b** and **c**, an absorbed layer (AL) is attached on the sample. x_0 is the middle of the sample, while x_1 and x_2 are the right side of RL and AL as noted in **a** and **b** respectively. x_3 is the left side of AL in **c**. **d**, **e** and **f**, are the V_{ISHE} detected in the Pt electrode when laser spot is scanned from $x=0$ on the surface of sample designed as **a**, **b**, and **c**, respectively. Insets of **e** and **f** are the enlarge view of green circle region to show the details of the curve change. The absorbed laser power is set to 30 mW for both lasers.

To distinguish the effects of thermal gradient and photo excitation on magnon diffusion, we selected a short wavelength (405 nm) and a long wavelength (808 nm) laser for further investigations. As show in Fig. 2a, we first covered a part of the Pt bar and the YIG film by an aluminum foil, which acts as reflected layer (RL) for incident light, and then repeated the experiments (to avoid short circuiting, an insulating sheet was inserted between RL and Pt). When the laser is focused on the region covered by the RL, a weak V_{ISHE} is observed. It can be ascribed to the simple thermal effect; absorption of the incident light by the RL caused a temperature growth of the RL and then a thermal gradient in underneath YIG, driving a magnon current.

Due to the high thermal conductivity of the RL, the thermal gradient could be uniform in YIG. Therefore, V_{ISHE} is independent of the position of the laser spot. When the light spot moves out of the right edge of the RL ($x=0.5$ mm), however, V_{ISHE}^{405} drops immediately to zero but V_{ISHE}^{808} jumps to a higher value before a slow exponential decaying with the distance from the Pt bar. The null V_{ISHE}^{405} means that the corresponding magnons are unable to reach the Pt bar by diffusion when they are 0.5 mm away from the right side of Pt bar. However, the magnons excited by the light of 808 nm can transport an obviously longer distance than 0.5 mm, and then are collected by Pt. This result indicates that the thermal effects of the two lights are similar but the excitation effects are different.

In the above paragraph, the irradiated RL generated a uniform thermal gradient. We also studied the effects of local thermal gradient. Magnons thus generated are called as pure thermal magnon. As shown in Fig. 2b, a black insulating absorb layer (AL) was used to cover the Pt bar and the YIG film. The absorbed energy by AL can be directly transferred to the YIG film when AL is illuminated, generating a V_{ISHE} as shown in Fig. 2e. Since the thermal conductivity of the AL is low, the maximal thermal gradient will appear exactly underneath the laser spot. As expected, V_{ISHE} is the highest at $x=0$, and rapidly decreases as laser spot moves along x -axis. Notably, the short and long wavelength lasers produce similar V_{ISHE-x} dependences as long as the laser spot locates on AL. This result implies that the thermal magnons produced by thermal gradient are the same in nature, regardless of the heating source. Here V_{ISHE}^{405} does not sharply drop to zero like in Fig. 1c when the laser spot leaves the Pt bar; the thermal energy will laterally expands inside AL, broadening the region with thermal gradient. Fascinatingly, as soon as the light spot completely leaves the AL, a sudden jump happens to V_{ISHE}^{808} , whereas V_{ISHE}^{405} keeps low, without any anomalous variation. Placing the AL so distant from the Pt (Fig. 2c) that the thermally excited magnon cannot reach the position of the Pt bar, we observed null V_{ISHE} as laser spot sweeps through the AL. However, when the laser spot gets out of the left edge of the AL, V_{ISHE}^{808} becomes nonzero immediately while V_{ISHE}^{405} remains null until the light spot is close enough to Pt. Again, long wavelength light shows its advantage over the

short one in generating long-diffusion-distance magnons. Based on the above results, we come to the conclusion that the diffusion length of thermal magnon generated by infrared light is much longer than the one induced by visible light and also the one by a simple thermal gradient.

As a supplement, we would like to point out that ultra-long diffusion length ξ^{808} has nothing to do with in-plane thermal gradient. Since the absorbed energy is identical for both lasers (30 mW), it will generate the same lateral thermal gradient, thus the same spatial evolution of V_{ISHE}^{808} and V_{ISHE}^{405} if the V_{ISHE-x} relation is determined by the lateral thermal gradient which is not the case in Fig. 2.

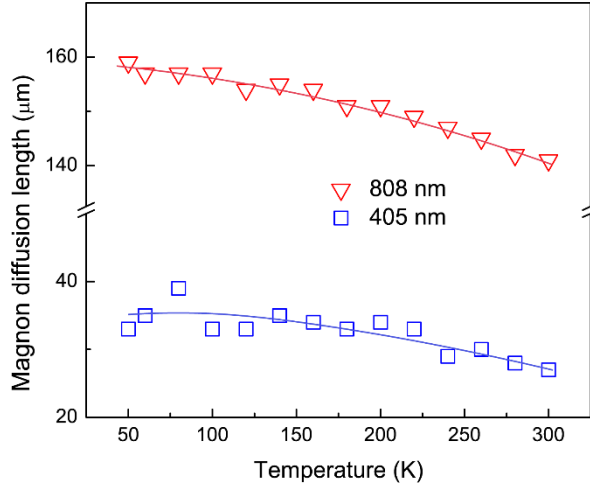


Figure 3 | Temperature dependence of thermal magnon diffusion length. The laser power is fixed at 30 mW.

A further issue is the temperature dependence of the diffusion distance of magnons. According to the Bose-Einstein distribution, the amount of thermal magnons and phonons will decrease with decreasing temperature. This means that the scattering between magnon and phonon will be weakened, and the diffusion distance will be increased. Guo *et al.*²³ found that $\xi \propto T^{-1}$, i.e., diffusion length is closely related to the number of phonons and magnons. On the contrary, a pervious study with nonlocal geometry found a slight reduction of ξ with decreasing temperature, and ascribed this phenomenon to a compensation effect of increased relaxation time by reduced thermal velocity of the magnon¹⁴. However, Fig. 3 shows that both ξ^{405} and ξ^{808} are only slightly increased upon cooling, rather than proportional to T^{-1} or slightly

decreasing. The different ζ - T dependence in Fig. 3 implies that the diffusion behavior of the non-equilibrium magnon induced by light irradiation is unique.

We also performed the same investigations for the thinner YIG film prepared by the PLD technique (40 nm). We found comparable diffusion length to that in LPE YIG (Supplementary Fig. S4). This result indicates that the difference in diffusion distance for the magnons induced by different lights is a general feature for YIG. This result is consistent with the report that the magnon transport along film plane is independent of film thickness²².

Our observation cannot be ascribed to the so called photo-spin-voltaic effect. A recent study²⁴ showed that when the Pt/YIG hybrid structure is exposed to light, especially infrared light, a photon-driven spin-dependent electron excitation will occur near the Pt-YIG interface, producing a photo-spin-voltaic effect. Since this effect is independent of the direction of temperature gradient, reversing the direction of thermal gradient will not change its sign. We reversed the incident direction of the light ($\lambda=808$ nm) and found a sign change of V_{ISHE} (Supplementary Fig. S5). Illuminating the back side of the sample, moreover, we observed the same magnon diffusion length as illuminating the front side (Supplementary Fig. S5). All these show that the V_{ISHE} detected here is unambiguously generated by non-equilibrium magnons instead of the photo-spin-voltaic effect.

To show what has happened to the illuminated YIG, we measured the absorption spectrum of YIG as shown in Fig. 4. According to earlier researches^{21, 28}, the peak around 800-1000 nm in the absorption spectrum arising from the ${}^6A_{1g}({}^6S) \rightarrow {}^4T_{1g}({}^4G)$ transition of the electron configuration in octahedral crystal field^{18, 19}, while the 650, 532, and 405 nm are corresponding to the ${}^6A_1({}^6S) \rightarrow {}^4T_1({}^4G)$, ${}^6A_1({}^6S) \rightarrow {}^4T_2({}^4G)$, and ${}^6A_1({}^6S) \rightarrow {}^4T_2({}^4D)$ transitions in the tetrahedral crystal field, respectively. Visible light may also be absorbed by the electron in octahedral crystal field. However, due to the octahedral symmetry, transitions between the ground state and any excited states are parity forbidden. As a result, the visible light is nearly totally absorbed by the electron in tetrahedral crystal field. It is well known that, two of the five Fe^{3+} ions in YIG are octahedrally coordinated (a sites) while other three are tetrahedrally coordinated (d

sites), forming two sublattices. YIG has the space group of $O_h^{10}-Ia3d$, and the tetrahedral and octahedral sublattices are distorted, having the point groups of $\bar{4}$ and $\bar{3}$, respectively. Y^{3+} is a nonmagnetic ion. The magnetic moments of the two sublattices arrange in antiparallel, i.e., the YIG is ferrimagnetic: The magnetic moment of the a -site (d -site) Fe^{3+} is antiparallel (parallel) to external magnetic field as well as the net magnetization. As well established, the superexchange constant J_{ad} is much larger than J_{aa} and J_{dd} ²⁵. The free-ion energy levels of the $3d^5$ configuration split in crystal field. The crystal field strength at a sites is at least twice as large as that at the d sites²⁶. As a result, the ${}^4T_{1g}({}^4G)$ state in octahedral crystal field is lower in energy than the ${}^4T_1({}^4G)$ and ${}^4T_2({}^4G)$ states in tetrahedral crystal field.

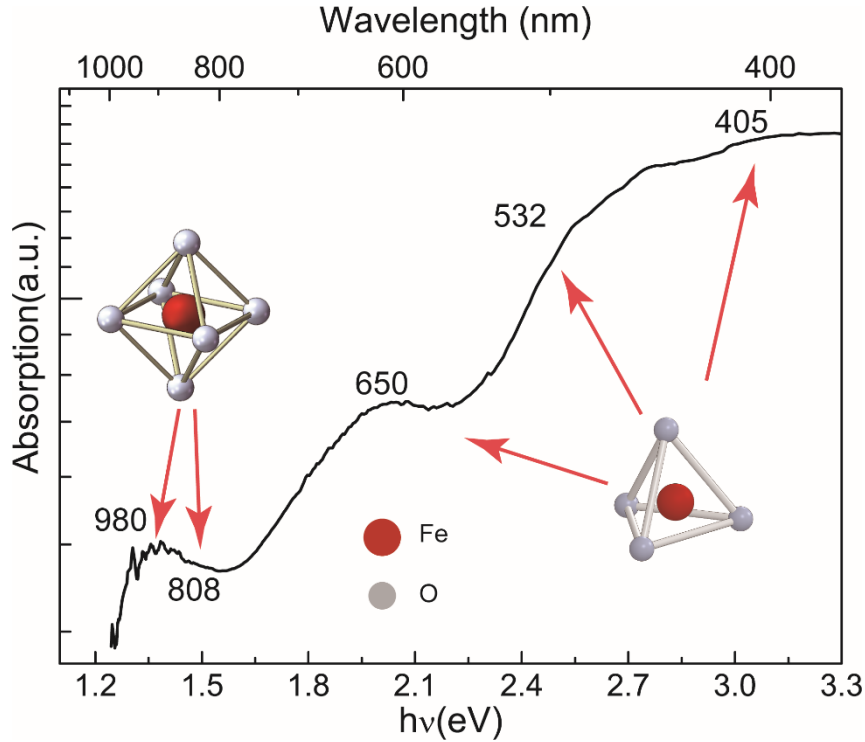


Figure 4 | Absorption spectrum of YIG prepared by PLD.

To reveal the underlying physics of the unusual diffusion behavior of the photo excited magnons, we performed a simple analysis of the factors that affect the kinetic behavior of the magnons. Ignoring the influence of J_{aa} and J_{dd} , we have the dispersion relation of the acoustic branch spin wave²⁷

$$\hbar\omega_k = 4|J_{ad}|a^2 \frac{S_d S_a}{S_d - S_a} k^2, \quad (2)$$

for a ferrimagnetic material with cubic crystal system under long wavelength approximation, where a , ω_k and k are respectively lattice constant, the frequency and wave vector of the magnon. S_a and S_d are the spin quantum number of the Fe^{3+} ions on a and d sites.

Obviously, the relaxation process will cause a dissipation of the magnons. The relaxation time τ has been calculated in many works^{28,29}. Following the procedure in Ref²⁸, it can be proven $\tau \sim D^{-1}$, where $D=4|J_{ad}|a^2 \frac{S_d S_a}{S_d - S_a}$, in this case, is the stiffness constant of the magnon. There is a simple relation between diffusion length and the stiffness constant $\xi \propto D^{-0.5}$, adopting the relation $\xi \propto \tau^{0.5}$. Therefore, if the variation of D with the electron configuration transition is known, the diffusion behavior of the magnons would be understood.

A simple analysis shows that a direct consequence of the ${}^6\text{A}_{1g} \rightarrow {}^4\text{T}_{1g}$, ${}^6\text{A}_1 \rightarrow {}^4\text{T}_1$, , and ${}^6\text{A}_1 \rightarrow {}^4\text{T}_2$ switching is spin state transition; the number on the upper left corner of each symbol is $2S+1$, with S being the spin angular quantum number of Fe^{3+} . The ground state and the excited state are a high-spin state and a low-spin state, respectively. When the spin state of the Fe^{3+} ion at a site (d site) changes from high spin state to low spin state under illumination, it will cause a reduction of S_a (S_d) from $5/2$ to $3/2$, thus a decrease (increase) in $\frac{S_d S_a}{S_d - S_a}$ or, equivalently, a softening (hardening) of the magnons. In addition to $\frac{S_d S_a}{S_d - S_a}$, J_{ad} is also a factor affecting the dispersion relation. According to Anderson³⁰, J_{ad} is proportional to Δ^{-2} , where $\Delta = E_d - E_p$, is the energy difference between the d and p orbital states of the magnetic ion and the oxygen ion, respectively. The energy splitting of the $3d^5$ state is strongly dependent on the configuration of the surrounding oxygen ions. E_d will grow when the electron transfer from the ${}^6\text{A}_{1g}({}^6\text{S})$ to the ${}^4\text{T}_{1g}({}^4\text{G})$ configuration, causing a decrease in J_{ad} . For the tetrahedral crystal field, according to Eq. (2) the effects of the spin state transition and the variation of J_{ad} counteract each other. For the octahedral crystal field, on the contrary, the two effects enhance each other, making the magnons softened.

From the absorption spectrum in Fig. 4, the lights of 808 nm and 980 nm affect only octahedral site Fe³⁺ (*a* site) while the visible light mainly influence tetrahedral site Fe³⁺ (*d* site). Based on the above analysis, the former process produces softer magnons than the latter one. According to the relation $\xi \propto D^{-0.5}$, soft magnons will have a long diffusion distance. Therefore, the magnon diffusion can be selectively tuned the electron configuration of Fe³⁺ ion.

It is worth mentioning that the lateral magnon diffusion length deduced from the nonlocal geometry could be substantially different from the diffusion length derived from local configuration. In the latter case the spin current is parallel to temperature gradient, thus suffers from the scattering of surface and interface^{8, 23}. As proven by recent investigations, the SSE mainly originated from long-wavelength magnons^{31, 21, 32}. Therefore, the magnons detected here are mainly long-wavelength ones. This is one of the reasons why the diffusion distance here is longer than that determined by other techniques such as Brillouin scattering which takes thermal magnons of the whole spectrum into account. The thermal magnon studied in this work presents a longer propagation length than the mean length of the thermal magnon of the whole spectrum⁹. We also noticed the experiment conducted by Gile *et al.*^{11, 17} The authors uses a Pt pad to generate thermal gradient and reported a diffusion length of 10 μm at 250 K. As demonstrated by our experiments (Fig. 2), the diffusion length is very short for magnons induced by thermal gradient alone, which is a conclusion consistent with that of Gile *et al.* Of cause, the incident light in the work of Gile *et al.* maybe also transmitted to YIG through the Pt pad. However, the Pt pad is 10 nm in thickness, and the transmitted intensity could be too weak to produce any significant effects.

Conclusion

In summary, we experimentally show that the diffusion length of the non-equilibrium magnon in YIG is strongly dependent on laser wavelength when they are induced by laser irradiation. Magnons generated by the laser beams of 808 nm and 980 nm can be detected from a distance as far as 1 mm. The corresponding diffusion lengths are 160 μm and 180 μm , respectively, while the diffusion lengths of the

magnons excited by visible light (400-650 nm) is only ~ 30 μm . We found unambiguous correspondences between the electron configuration and magnon diffusion. Long-wavelength laser excites a transition of the electron configuration for the FeO_6 octahedra in YIG and induces softened magnons which have a longer diffusion distance. In contrast, visible light only affects electron configuration in the FeO_4 tetrahedra, and the corresponding magnons are stiff. The present work demonstrates for the first time the tuning of magnon diffusion by selective modification of electron configuration. The principle proven here can be extended to other materials.

Acknowledgements

This work is supported by the National Natural Science Foundation of China (Nos. 11604265, 51402240, 11520101002 and 51572222) and the Fundamental Research Funds for the Central Universities (No. 3102017jc01001). J.R. Sun thanks the support of the National Basic Research of China (2016YFA0300701), and Key Program of the Chinese Academy of Sciences.

Author contributions

S.H. Wang conceived the idea, established the experimental setup and analyzed the data. G. Li, Y.Y. Tian, X.L. Zheng and L.K. Zou fabricated and characterized the sample together. S.H. Wang, J.Y. Wang, H. Yan, Z.T. Zhang and M. Wang performed the measurement. J.R. Sun, S.H. Wang, K.X. Jin, E.J. Guo, Y. Zhao and J.W. Cai provide the theoretical analysis. S.H. Wang and J.R. Sun wrote the paper and the supplementary information with help from all the other co-authors.

Reference

1. Uchida K, Adachi H, Ota T, Nakayama H, Maekawa S, Saitoh E. Observation of longitudinal spin-Seebeck effect in magnetic insulators. *Appl Phys Lett* **97**, 172505-172503 (2010).
2. Uchida K, Ishida M, Kikkawa T, Kirihara A, Murakami T, Saitoh E. Longitudinal

spin Seebeck effect: from fundamentals to applications. *J Phys-Condens Mat* **26**, (2014).

3. Magginietti D, Tian K, Tiwari A. β -Tantalum, a better candidate for spin-to-charge conversion. *Solid State Communications* **249**, 34-37 (2017).
4. Jiang Z, *et al.* Enhanced spin Seebeck effect signal due to spin-momentum locked topological surface states. *Nat Commun* **7**, (2016).
5. Ramos R, *et al.* Observation of the spin Seebeck effect in epitaxial Fe₃O₄ thin films. *Appl Phys Lett* **102**, 072413 (2013).
6. Seki S, *et al.* Thermal Generation of Spin Current in an Antiferromagnet. *Physical Review Letters* **115**, 266601 (2015).
7. Wu SM, Pearson JE, Bhattacharya A. Paramagnetic Spin Seebeck Effect. *Physical Review Letters* **114**, (2015).
8. Kehlberger A, *et al.* Length Scale of the Spin Seebeck Effect. *Physical Review Letters* **115**, (2015).
9. An K, *et al.* Magnons and Phonons Optically Driven out of Local Equilibrium in a Magnetic Insulator. *Physical Review Letters* **117**, 107202 (2016).
10. Cornelissen LJ, Liu J, Duine RA, Youssef JB, van Wees BJ. Long-distance transport of magnon spin information in a magnetic insulator at room temperature. *Nat Phys* **11**, 1022-1026 (2015).
11. Giles BL, Yang Z, Jamison JS, Myers RC. Long-range pure magnon spin diffusion observed in a nonlocal spin-Seebeck geometry. *Physical Review B* **92**, 224415 (2015).
12. Shan J, Cornelissen LJ, Liu J, Youssef JB, Liang L, Wees BJv. Criteria for accurate determination of the magnon relaxation length from the nonlocal spin Seebeck effect. *arXiv:170906321* (2017).
13. Shan J, *et al.* Influence of yttrium iron garnet thickness and heater opacity on the nonlocal transport of electrically and thermally excited magnons. *Physical Review B* **94**, 174437 (2016).
14. Cornelissen LJ, Shan J, van Wees BJ. Temperature dependence of the magnon spin diffusion length and magnon spin conductivity in the magnetic insulator yttrium iron garnet. *Physical Review B* **94**, 180402 (2016).
15. Huang SY, *et al.* Transport magnetic proximity effects in platinum. *Phys Rev Lett* **109**, 107204 (2012).
16. Lu YM, *et al.* Pt Magnetic Polarization on Y₃Fe₅O₁₂ and Magnetotransport Characteristics. *Physical Review Letters* **110**, 147207 (2013).
17. Giles BL, *et al.* Thermally Driven Long Range Magnon Spin Currents in Yttrium Iron Garnet due to Intrinsic Spin Seebeck Effect. *arXiv:170801941* (2017).
18. Scott GB, Lacklison DE, Page JL. Absorption spectra of Y₃Fe₅O₁₂ (YIG) and Y₃Ga₅O₁₂: Fe³⁺. *Physical Review B* **10**, 971-986 (1974).
19. Wemple SH, Blank SL, Seman JA, Biolsi WA. Optical properties of epitaxial iron garnet thin films. *Physical Review B* **9**, 2134-2144 (1974).
20. Aqeel A, Vera-Marun IJ, Wees BJv, Palstra TTM. Surface sensitivity of the spin Seebeck effect. *Journal of Applied Physics* **116**, 153705 (2014).
21. Kikkawa T, Uchida K-i, Daimon S, Qiu Z, Shiomi Y, Saitoh E. Critical suppression of spin Seebeck effect by magnetic fields. *Physical Review B* **92**, 064413 (2015).
22. Liu J, Cornelissen LJ, Shan J, Kuschel T, van Wees BJ. Magnon planar Hall effect

and anisotropic magnetoresistance in a magnetic insulator. *Physical Review B* **95**, 140402 (2017).

23. Guo E-J, *et al.* Influence of Thickness and Interface on the Low-Temperature Enhancement of the Spin Seebeck Effect in YIG Films. *Physical Review X* **6**, 031012 (2016).

24. Ellsworth D, *et al.* Photo-spin-voltaic effect. *Nat Phys* **12**, 861-866 (2016).

25. Anderson EE. Molecular Field Model and the Magnetization of YIG. *Phys Rev* **134**, A1581-A1585 (1964).

26. McClure DS. *Electronic Spectra of Molecules and Ions in Crystals: Part I. Molecular Crystals. Part II. Spectra of Ions in Crystals.* Academic Press (1959).

27. Van Kranendonk J, Van Vleck JH. Spin Waves. *Rev Mod Phys* **30**, 1-23 (1958).

28. Braggio C, Carugno G, Guarise M, Ortolan A, Ruoso G. Optical Manipulation of a Magnon-Photon Hybrid System. *Physical Review Letters* **118**, 107205 (2017).

29. Woods LM. Magnon-phonon effects in ferromagnetic manganites. *Physical Review B* **65**, 014409 (2001).

30. Anderson PW. Antiferromagnetism. Theory of Superexchange Interaction. *Phys Rev* **79**, 350-356 (1950).

31. Jin H, Boona SR, Yang Z, Myers RC, Heremans JP. Effect of the magnon dispersion on the longitudinal spin Seebeck effect in yttrium iron garnets. *Physical Review B* **92**, 054436 (2015).

32. Boona SR, Heremans JP. Magnon thermal mean free path in yttrium iron garnet. *Physical Review B* **90**, 064421 (2014).